Fluorescence imaging of amyloid formation in living cells by a functional, tetracysteine-tagged α-synuclein

María J Roberti[1,2], Carlos W Bertoncini[1], Reinhard Klement[1], Elizabeth A Jares-Erijman[2] & Thomas M Jovin[1]

α-synuclein is a major component of intraneuronal protein aggregates constituting a distinctive feature of Parkinson disease. To date, fluorescence imaging of dynamic processes leading to such amyloid deposits in living cells has not been feasible. To address this need, we generated a recombinant α-synuclein (α-synuclein-C4) bearing a tetracysteine target for fluorogenic biarsenical compounds. The biophysical, biochemical and aggregation properties of α-synuclein-C4 matched those of the wild-type protein *in vitro* and in living cells. We observed aggregation of α-synuclein-C4 transfected or microinjected into cells, particularly under oxidative stress conditions. Fluorescence resonance energy transfer (FRET) between FlAsH and ReAsH confirmed the close association of fibrillized α-synuclein-C4 molecules. α-synuclein-C4 offers the means for directly probing amyloid formation and interactions of α-synuclein with other proteins in living cells, the response to cellular stress and screening drugs for Parkinson disease.

Parkinson disease is the most common motor-neurodegenerative disease, arising from a degeneration of dopaminergic neurons in the midbrain, attributable at least in part to mitochondrial dysfunction and compromised ubiquitin-proteasomal activity[1,2]. Intraneuronal protein aggregates (Lewy bodies[3]) are pathognomonic of idiopathic Parkinson disease, but it is still unclear whether such structures are in themselves pathogenic[2] or have a protective role by sequestering cytotoxic protein oligomers[4,5]. Ultrastructurally, Lewy bodies exhibit amyloid-like fibrils composed mainly of α-synuclein along with other proteins such as ubiquitin, neurofilaments and tubulin. α-synuclein is a natively unfolded 140-amino-acid presynaptic protein[6,7] whose fibrillation *in vitro* occurs via a nucleation-propagation mechanism modulated by many factors such as polycations (for example, spermine) and aberrant phosphorylation[8,9]. Under pathological conditions, glial cells also show cytoplasmatic α-synuclein deposits[10]. Cellular and rodent models of Parkinson disease display neuronal loss accompanying the formation of reactive oxygen species (ROS), and the appearance of aggregates immunoreactive for α-synuclein and ubiquitin[11,12].

The successful application of fluorescence techniques in studies of α-synuclein oligomerization and aggregation in living cells has been an elusive goal, although aggregates in fixed cells can be imaged through immunofluorescence or amyloid-reporting dyes such as Thioflavin-T (ThioT) and Thioflavin-S (ThioS)[13]. Fluorescent proteins fused to proteins related to other neuropathologies featuring deposits (for example, poly-Q fragments associated with Huntington disease), yield fluorescent aggregates in cells[14,15]. Some reports of GFP derivatives of α-synuclein demonstrated aggregation in cells[16–18], but other attempts either with α-synuclein or other small proteins such as the Alzheimer disease–related Aβ-peptide produced abnormal, nonfluorescent aggregates, indicating that the ∼27 kDa of a fluorescent protein can perturb the native properties of the target protein (∼15 kDa for α-synuclein)[19]. None of the cited studies validated the constructs by comparing their properties *in vitro* to those of native α-synuclein.

A general tagging strategy based on the introduction of small (∼1.5 kDa) tetracysteine-motif fusion peptides as specific targets for externally applied biarsenical fluorogenic compounds, overcomes such limitations. Biarsenical labeling[20] has proven effective for monitoring many real-time processes *in vitro* and within cells[21,22]. In the present work, we engineered α-synuclein-C4 (tetracysteine-tagged version of α-synuclein) by fusing a 12-mer peptide (FLNCCPGCCMEP[23], denoted P12) to the C-terminal region of the protein. Extensive characterization of the properties of α-synuclein-C4 *in vitro* revealed no apparent differences between the modified and the wild-type protein. Biarsenical labeling permitted the monitoring of α-synuclein aggregation both *in vitro* and in living cells, and fluorescence microscopy established the intracellular distribution of singly labeled (FlAsH) α-synuclein-C4. We performed immunological assays in cells, and compared biarsenical labeling and antibody staining[24] as indicators of aggregation, which was enhanced by the application of oxidative stress. We assessed the degree of self-association of α-synuclein-C4 in inclusions by FRET between FlAsH and ReAsH.

To our knowledge, we provide here the first rigorously tested fluorescence labeling system for α-synuclein capable of resolving details of the molecular mechanisms underlying protein oligomerization and aggregation in cells. This method may also apply to amyloid peptides and proteins associated with other neuropathologies.

[1]Department of Molecular Biology, Max Planck Institute for Biophysical Chemistry, 37077 Göttingen, Germany. [2]Departamento de Química Orgánica, Facultad de Ciencias Exactas y Naturales, Universidad de Buenos Aires, 1428 Buenos Aires, Argentina. Correspondence should be addressed to E.A.J.-E. (eli@qo.fcen.uba.ar) or T.M.J. (tjovin@gwdg.de).

Figure 1 | Characterization of tetracysteine-tagged α-synuclein-C4. (**a**) Structure of α-synuclein-C4–FlAsH, adapted from an NMR-derived model for an ensemble of α-synuclein conformations. The P12-FlAsH complex is highlighted, showing the FlAsH molecule (purple), the tetracysteine tag (yellow) and the flanking residues of the tag (green); the protein backbone is represented as the 5% amplitude isosurface of the density of atoms in the polypeptide chain (gray). (**b**) SDS-PAGE of a FlAsH-labeled bacterial lysate expressing α-synuclein-C4, exposed to UV light for FlAsH excitation (left) and then stained with coomassie blue (right). (**c**) SDS-PAGE of purified α-synuclein-C4–FlAsH (left) and α-synuclein-C4–ReAsH (right lane) exposed to UV light. (**d**) SDS-PAGE of decreasing amounts of α-synuclein-C4–ReAsH (amount indicated in micrograms) detected by ReAsH fluorescence (left) and western blotting (right). (**e**) Plot of mean weighted NMR ^{1}H-^{15}N chemical shift differences between α-synuclein-C4 and α-synuclein (blue), and between α-synuclein-C4–FlAsH and α-synuclein (green). Dashed lines delineate the 0.02 p.p.m threshold. The addition of the tetracysteine tag does not perturb α-synuclein structure. (**f**) Fluorescence spectra of α-synuclein-C4–FlAsH and α-synuclein-C4–ReAsH in microinjected HeLa cells using the SpectraCube system[26]: normalized emission of FlAsH and ReAsH in aggregated (green and red curves, respectively) and nonaggregated (blue and orange curves, respectively) regions. (**g**,**h**) Intracellular regions imaged during the acquisition of spectra, with aggregated (arrow) and nonaggregated (box) α-synuclein-C4–FlAsH (**g**) and α-synuclein-C4–ReAsH (**h**). Scale bars, 10 μm.
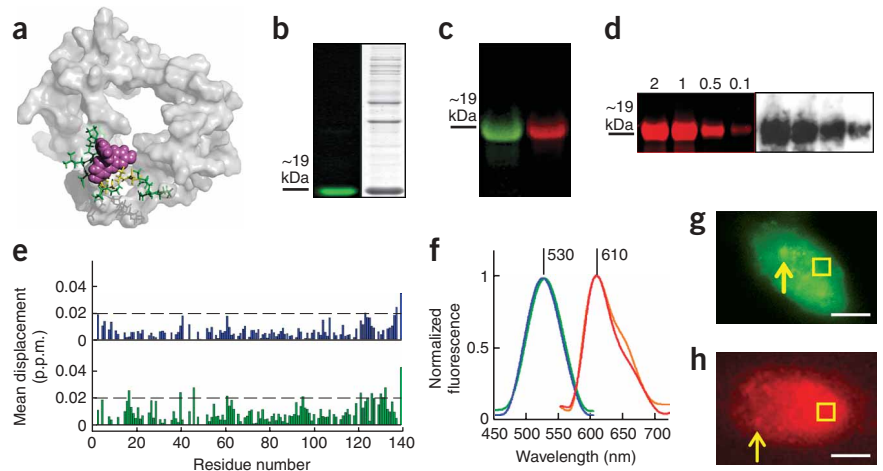
RESULTS

Generation and characterization of α-synuclein-C4

The protective long-range interactions that maintain α-synuclein in an auto-inhibited state involve a precise interplay between key residues at the C terminus and other amino acids far apart in the primary sequence[7]. A hydrophobic cluster involving Met116, Pro117, Val118, Ala124 and Tyr125 appears to act as a sensitive electrostatic gate for initiating α-synuclein aggregation. Amyloid formation is triggered, for example, by phosphorylation of Tyr125 or Ser129 (addition of negative charge in the hydrophobic pocket), and binding of polyamines (addition of positive charge) to the region 120–130. P12 fused to the C terminus of α-synuclein is small, almost uncharged (charge, −1) and located 15–20 residues away from the key interaction loci. Furthermore, the C terminus of α-synuclein is not incorporated into the fibrillar core and remains disordered[25], thus avoiding substantial perturbations of the self-oligomerization and fibrillation properties of the protein. A structural model of α-synuclein-C4 (**Fig. 1a**) based on an ensemble of nuclear magnetic resonance (NMR)-generated conformations of α-synuclein[7] confirmed that the presence of P12 complexed with FlAsH should not perturb the native state of the protein.

α-synuclein-C4 expressed well in *Escherichia coli*. An aliquot of the bacterial lysate stained with FlAsH and analyzed by SDS-PAGE, revealed a single fluorescent band at ∼19 kDa (**Fig. 1b**) comigrating with reference α-synuclein, and testifying to the high specificity of FlAsH for the tetracysteine tag. Aliquots of purified α-synuclein-C4 labeled with FlAsH or ReAsH also displayed a single fluorescent band at ∼19 kDa (**Fig. 1c**). Western blotting confirmed the identity of the protein and showed the high sensitivity (∼0.1 μg detection limit) for α-synuclein-C4 detection attainable with ReAsH (**Fig. 1d**) or FlAsH (data not shown). Mass spectrometry performed on α-synuclein-C4 indicated that the entire recombinant protein sequence was expressed (*m/z*, 15,912 Da).

NMR spectroscopy and size-exclusion chromatography served to evaluate changes in the native conformation of monomeric α-synuclein upon fusion to P12. A comparison of the mean weighted chemical shifts (**Fig. 1e** and **Supplementary Fig. 1** online) showed unaltered values (<0.02 p.p.m.) up to residue Glu139 in the ^{1}H-^{15}N heteronuclear single quantum correlation (HSQC) spectra of α-synuclein-C4 and α-synuclein-C4–FlAsH relative to α-synuclein. By size-exclusion chromatography, the hydrodynamic states of the recombinant protein alone and bound to FlAsH or ReAsH corresponded to that of the wild-type (see elution times and peak profiles in **Supplementary Fig. 2** online).

The excitation and emission peaks for α-synuclein-C4–FlAsH were at 510 nm and 530 nm, respectively, with corresponding values for α-synuclein-C4–ReAsH at 595 nm and 610 nm. In both cases, the normalized spectra of the labeled protein matched those obtained for labeled P12, and the same was true for the corresponding spectra of protein aggregates obtained *in vitro* (data not shown). We assessed the emission properties inside HeLa cells by fluorescence microscopy after introducing the labeled protein by microinjection. Using an interferometric spectral image analyzer[26], we obtained an emission spectrum for each pixel. There were no observable differences between the emission spectra of α-synuclein-C4–FlAsH (or α-synuclein-C4–ReAsH) in aggregated and nonaggregated regions within cells, and emission maxima matched those obtained *in vitro* (**Fig. 1f–h**). These results suggest that the spectral properties of FlAsH and ReAsH complexed with α-synuclein-C4 are governed mainly by the environment provided by P12 and are unaffected by the conformational state of α-synuclein-C4.

α-synuclein-C4 fibrillation *in vitro*

We compared the fibrillation propensity of α-synuclein-C4 and the wild-type protein using the standard ThioT fluorescence assay. Both proteins showed comparable half-life ($t_{1/2}$) values (α-synuclein-C4, 79 ± 4 h; α-synuclein, 77 ± 3 h; in the presence of spermine[27], α-synuclein-C4, 36 ± 4 h; α-synuclein, 34 ± 3 h; **Fig. 2a**). Formation of the complex with ReAsH had no effect on $t_{1/2}$ (76 ± 2 h; **Fig. 2b**). FlAsH emission interfered with the

ThioT signal such that the latter could not report on α-synuclein-C4–FlAsH aggregation. During aggregation, the fluorescence of the labels remained constant (**Fig. 2b**).

We investigated the structure of fibrillated α-synuclein-C4 alone, and bound to FlAsH and ReAsH by atomic force microscopy (AFM) and confocal fluorescence microscopy (**Fig. 2c–f**). The AFM samples contained fibrils with lengths of 0.1–1.5 μm. Confocal microscopy revealed the typical features previously observed for α-synuclein aggregates stained with ThioT[9], but the inherent limited spatial resolution of the technique did not suffice for observation of individual fibrils.

We successfully labeled aggregated α-synuclein-C4 (**Fig. 2e**), attesting to the accessibility to the external medium of the tetracysteine tag. We established the absence of segregation between α-synuclein and α-synuclein-C4 by incubating aggregates of wild-type protein with α-synuclein-C4–FlAsH monomer. After 8 h, confocal microscopy revealed the α-synuclein-C4–FlAsH signal throughout the structures (**Fig. 2f**). Control samples consisting of aggregates of wild-type mixed briefly (~15 min) with α-synuclein-C4–FlAsH were nonfluorescent, indicating the absence

Figure 2 | α-synuclein-C4 aggregation *in vitro*. (**a**) Normalized aggregation curves showing the evolution of α-synuclein-C4 and α-synuclein with and without spermine. Each data point is an average of duplicate samples. (**b**) Normalized aggregation kinetics of α-synuclein-C4–ReAsH and α-synuclein. Temporal evolution of ReAsH fluorescence in α-synuclein-C4–ReAsH. (**c**) Atomic force microscopy of fibrils obtained after a standard *in vitro* aggregation assay (top, α-synuclein-C4; bottom, wild-type α-synuclein). Scale bars, 0.5 μm. (**d**) Fluorescence confocal images of α-synuclein-C4–FlAsH aggregates showing the morphology along the structure (stack interval in the axial direction z, 2 μm). (**e**) Confocal section of aggregated protein obtained from incubation of α-synuclein-C4 monomer and stained with FlAsH. The tetracysteine tag is accessible to FlAsH in the interior of α-synuclein-C4 aggregates. (**f**) Compatibility in the interaction between α-synuclein-C4 and α-synuclein, demonstrated by incubating α-synuclein aggregates with α-synuclein-C4–FlAsH monomer. FlAsH fluorescence was localized throughout the structures 8 h after incubation. Scale bars in **d**, **e** and **f**, 10 μm.

of unspecific interactions of the monomer. We conclude that there was neither an impediment nor a bias to the joint association or aggregation of α-synuclein and α-synuclein-C4.

Visualization of α-synuclein-C4 fibrillation in living cells

A first assessment of the behavior of α-synuclein-C4 in a cellular environment was by microinjection of purified α-synuclein-C4–FlAsH into HeLa cells (selected for their robustness and tolerance to microinjection), and imaging every 24 h over 3 d. Initially, α-synuclein-C4–FlAsH was distributed uniformly, and the daughter cells conserved the fluorescence (**Fig. 3a**). Discrete and approximately round accumulations with an intense FlAsH signal became first apparent after 48 h (**Fig. 3b**). Staining with the DNA dye Hoechst 33342 established that the cells were alive (**Fig. 3c**). Optical sections revealed that the aggregates were located in the cytoplasm and the perinuclear region, but not within the nucleus. Control cells microinjected with a solution of FlAsH alone did not exhibit aggregates. We confirmed the amyloid characteristics of the structures by ThioS staining of fixed cells microinjected with α-synuclein-C4–ReAsH; the simultaneous imaging of both labels showed colocalization in regions with aggregates (**Supplementary Fig. 3** online).

Immunological staining with an antibody to monomeric α-synuclein (BD-AB; **Supplementary Methods** online) detected the targeted protein throughout the cells (**Fig. 3d**), but the aggregates were only visible in the FlAsH channel.

Transfection in living SH-SY5Y cells and ROS induction

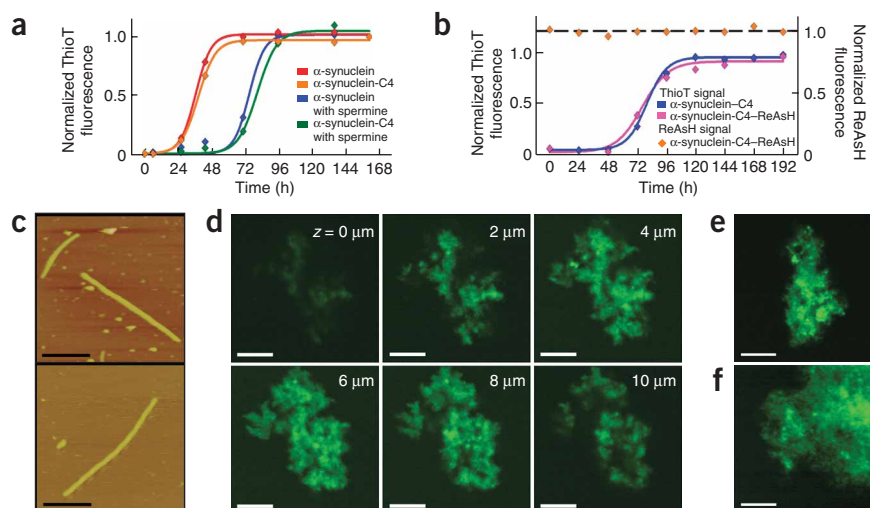We transiently transfected SH-SY5Y human neuroblastoma cells and stained them with FlAsH 48 h later. We achieved an expression efficiency of ~15% (determined by FlAsH fluorescence), and 10 ± 2% of the positively transfected cells exhibited highly fluorescent aggregates. We estimated the background signal with two controls, one consisting of nontransfected cells and another with cells transfected and expressing wild-type α-synuclein. In both cases the fluorescence was notably lower, that is, ~1/5 that of α-synuclein-C4–transfected cells.

Confocal microscopy showed predominantly spherical intracellular aggregates located in the perinuclear region, with diameters in the range of 0.5–2 μm (**Fig. 4a**); some aggregates were more elongated, (that is, lengths of up to 3 μm). A 3D projection from the z-stack scanning allowed the reconstruction of the spatial distribution of these structures within the cell (**Supplementary Video 1** online). The fluorescence signal corresponding to nonaggregated α-synuclein-C4 appeared in the nucleus and cytoplasm.

For immunological staining, we used two different α-synuclein antibodies, BD-AB (used in HeLa experiments) and Syn211-AB directed against amyloid aggregates and Lewy bodies[24] (**Supplementary Methods**). BD-AB revealed a homogeneous distribution of α-synuclein colocalized with the FlAsH signal but did not recognize aggregates (**Fig. 4b**). The detection of aggregates exclusively by FlAsH may reflect the greater accessibility of the tetracysteine tag to the biarsenicals compared to the epitopes targeted by BD-AB, as was observed with fibrils *in vitro*. Control cells transfected to express wild-type α-synuclein also showed a strong immunofluorescence signal comparable to that of α-synuclein-C4–transfected cells, but no aggregates (**Fig. 4b**). The antibody signal associated with the endogenous level of α-synuclein in nontransfected SH-SY5Y was lower but substantial. We repeated this assay using the Syn211-AB
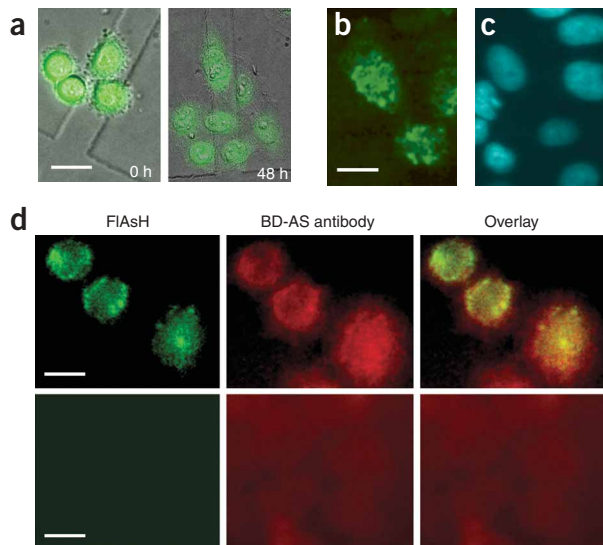
Figure 3 | Direct visualization of α-synuclein-C4 aggregation in microinjected HeLa cells by fluorescence microscopy. (**a**) Fluorescence images of HeLa cells microinjected with α-synuclein-C4–FlAsH 2 h (left) and 48 h (right) after microinjection. Scale bar, 30 μm. (**b,c**) α-synuclein-C4–FlAsH aggregates in living HeLa cells 48 h after microinjection (**b**), with the corresponding Hoechst staining (**c**) showing the integrity of the nuclei. Scale bar, 15 μm. (**d**) Immunological staining assay, 48 h after microinjection. FlAsH fluorescence (left), immunofluorescence signal (BD-AB primary antibody against monomeric α-synuclein, Alexa 633–conjugated secondary antibody; middle) and channel overlay (right). Scale bars, 20 μm.

antibody (**Fig. 4c**), which colocalized with α-synuclein-C4–FlAsH in regions corresponding to aggregates.

In previous studies performed on SH-SY5Y cells, the application of FeCl$_2$ promoted the formation of ROS and induced α-synuclein aggregation in cells overexpressing the protein[28]; the aggregates were revealed by immunological labeling. We sought to demon-strate the applicability of the recombinant α-synuclein-C4 for observing this effect in living cells. SH-SY5Y cells subjected to FeCl$_2$ treatment displayed an increase in the proportion of cells with α-synuclein-C4–FlAsH aggregates to 25 ± 4% of the positively transfected cells, a value that differed significantly from that for untreated cells (**Fig. 4d**). However, the number of aggregates per cell (a rather ambiguous quantity because of the inherent poly-morphic nature of such structures) was not substantially different between FeCl$_2$ treated or untreated cells; the localization and morphology of the aggregates were unaltered (**Fig. 4d**).

FRET studies on α-synuclein-C4 fibrillation

FRET-based microscopies applied to FlAsH and ReAsH bound to α-synuclein-C4 can report on intermolecular distances (r) in associated and aggregated forms of the protein, if donor (FlAsH)
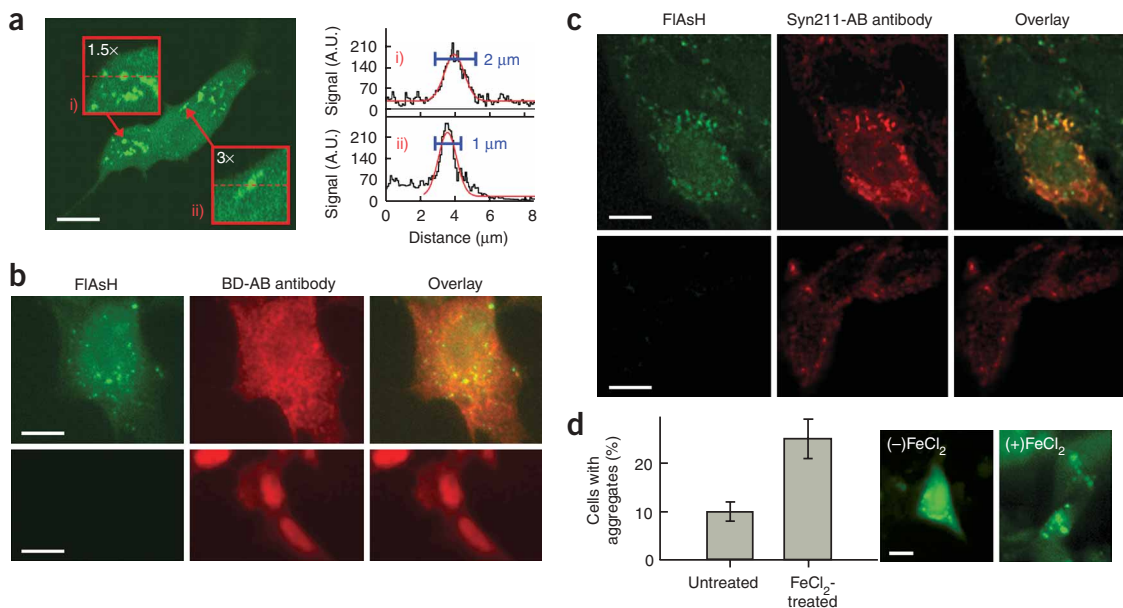

Figure 4 | Fluorescence imaging of α-synuclein-C4 aggregates in transfected SH-SY5Y cells; effect of oxidative stress. (**a**) Confocal microscopy of cells displaying α-synuclein-C4–FlAsH cytoplasmatic aggregates (stack interval, 0.5 μm). Scale bar, 10 μm. The sizes of the aggregates were estimated from measurements of the fluorescence intensity profile along the dashed red line (inside the red boxes with the amplified images), at the middle plane image of the z-sectioning. (**b**) Immunological staining assay of cells expressing α-synuclein-C4 (top; scale bar, 10 μm), and control cells transfected with and expressing wild-type α-synuclein (bottom; scale bar, 40 μm). FlAsH fluorescence (left), immunological staining (BD-AB primary antibody, Alexa 633–conjugated secondary antibody; middle) and channel overlay (right). (**c**) Immunological staining using Syn211-AB of cells expressing α-synuclein-C4 (top) and cells transiently transfected to express wild-type α-synuclein (bottom). FlAsH fluorescence and antibody signal (Alexa 633–conjugated secondary antibody) colocalize in regions with aggregates. Scale bars, 20 μm. (**d**) Oxidative stress triggered by FeCl$_2$ incubation induces α-synuclein-C4 aggregation. Percentage of cells showing aggregates for untreated and FeCl$_2$-treated cells (10 ± 2% and 25 ± 4%, respectively ($P < 0.05$)). Data are means ± s.e.m. of three independent experiments, calculated from the positively transfected cells (transfection efficiency ~15%, population size $n > 400$). Fluorescence images of α-synuclein-C4–FlAsH aggregates observed in living cells (right), untreated ((–)FeCl$_2$) and exposed to FeCl$_2$ ((+)FeCl$_2$), 72 h after transfection. Scale bar, 20 μm.
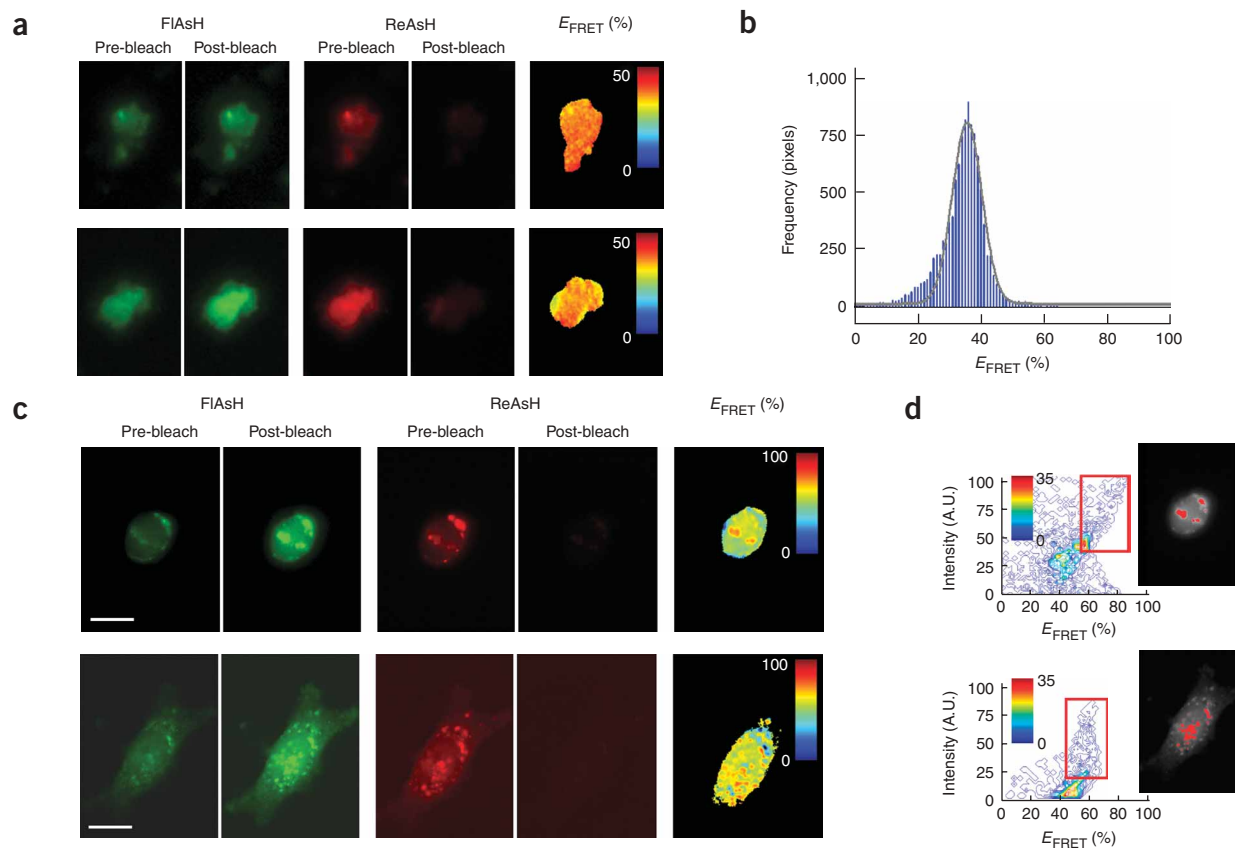
Figure 5 | Characterization of aggregated α-synuclein-C4 *in vitro* and in cells by apbFRET microscopy. (**a**) Determination of E_{FRET} in aggregates prepared from a 1:4 monomer mixture of α-synuclein-C4–FlAsH and α-synuclein-C4–ReAsH *in vitro*. FlAsH emission before and after ReAsH photobleaching (left), ReAsH emission channel before and after photobleaching (middle) and E_{FRET} map (right). (**b**) Histogram of the E_{FRET} values obtained from the set of aggregates (number of samples, $n = 5$), calculated on a pixel-to-pixel basis. The distribution was fitted to a Gaussian function, mean $E_{FRET} = 36\%$. (**c**) Living SH-SY5Y cells transiently expressing α-synuclein-C4, labeled with a 1:4 mixture of FlAsH and ReAsH. FlAsH emission channel before and after ReAsH photobleaching (left), ReAsH emission channel before and after photobleaching (middle) and E_{FRET} (right). Scale bars, 10 μm (top) and 20 μm (bottom). (**d**) Two-dimensional histogram of the correlation between FlAsH fluorescence intensity and E_{FRET}. For each sample, the values of the histogram within the red box were mapped back onto the FlAsH fluorescence image (right), to highlight the regions (red) that jointly displayed high FlAsH fluorescence and high E_{FRET}. The color scale bars represent frequency (number of pixels).

and acceptor (ReAsH) are in close proximity ($r < 1.5\ R_0$, the critical Förster distance). The calculated R_0 was 39 Å. We determined the FRET efficiency (E_{FRET}) by acceptor-photobleaching FRET (apbFRET) microscopy[29] (**Supplementary Methods**) of fibrils prepared *in vitro* and in transfected SH-SY5Y cells challenged with $FeCl_2$ to increase the proportion of aggregates.

We first characterized doubly labeled samples fibrillized *in vitro* (1:4 mixture of α-synuclein-C4–FlAsH and α-synuclein-C4–ReAsH). There was a distinct recovery of FlAsH fluorescence after selective photobleaching of ReAsH (**Fig. 5a**). The computed pixel-by-pixel E_{FRET} fitted well to a Gaussian with a mean of 36% (**Fig. 5b**), corresponding to a distance of $r < 5$ nm between neighboring tetracysteine tags and thus between the C termini of the aggregated α-synuclein-C4 molecules. The same mixture of monomers before aggregation had a mean $E_{FRET} < 5\%$, indicating a lack of substantial interaction. Fibrils labeled exclusively with FlAsH showed a negligible ($<3\%$) loss of the label under the conditions used for photobleaching ReAsH.

For the experiments with SH-SY5Y cells expressing the recombinant protein, we performed the biarsenical labeling with a 1:4 mixture of FlAsH and ReAsH, 48 h after transfection. The

pixel-by-pixel E_{FRET} values were 10–80%, with high variability between cells (**Fig. 5c**). Thus, a single mean E_{FRET} was not appropriate for depicting the actual distribution of the values inside the cell. To address this issue, we plotted the pixel-by-pixel correlation between E_{FRET} and signal intensity as two-dimensional histograms (**Fig. 5d**). We identified two clearly defined regions, one rich in aggregated protein displaying high E_{FRET} values between 60 and 80%, and another corresponding to the nonaggregated protein, with an E_{FRET} between 30 and 45%. These segmented regions of the two-dimensional histograms, backmapped to the original intensity images, identified the two compartments.

DISCUSSION

It is widely reported that many factors can perturb α-synuclein, leading to neurotoxic aggregation-prone states[8,9,18]. Our α-synuclein-C4 construct retained the native characteristics and intrinsic aggregation properties of α-synuclein *in vitro* and appears to be a reliable reporter of the association and aggregation phenomena attributable to the native protein. The spectroscopic properties of the probes remained unchanged during aggregation, reflecting the stability and invariant solvent exposure of the

protein-ligand complex despite the presumed conformational changes (adoption of a β-sheet secondary structure) in the core of the protein. Confocal imaging revealed that α-synuclein-C4 and α-synuclein were intermixed in fibrils, an indication of their equivalent functionality. The limitations in the fluorescence imaging of individual fibrils may soon be circumvented by using more refined imaging techniques such as super-resolution stimulated emission depletion (STED)[30] and single-molecule microscopies. Also, we can anticipate that the fluorescent features of α-synuclein-C4–FlAsH applied in kinetic studies of fibril growth will provide new insights about α-synuclein association at the molecular level.

Microinjection of α-synuclein-C4–FlAsH provided a link between studies in vitro and biarsenical labeling in cells, by making possible to compare the features of the purified protein characterized in vitro and microinjected, with those observed by transient transfection and exogenous labeling. Both strategies led to clustering of fluorescent signals indicative of local α-synuclein aggregation, with similar morphology, intracellular localization and amyloid characteristics. The fact that the imaging could be performed over extended periods of time (days) attested to the viability of the cells[23]. The sensitivity for detecting aggregates achieved with biarsenical labeling was comparable to that of an antibody directed against Lewy bodies, and the colocalization of the two probes confirmed the amyloid characteristics of the deposits.

E_{FRET} mapping confirmed the highly aggregated nature of aggregates in vitro and also provided a reference value for the mean distance between α-synuclein molecules in such structures. The E_{FRET} values for aggregates within cells achieved maximal values higher than the mean value in vitro, demonstrating a greater degree of heterogeneity in the intracellular structures. Additionally, the aggregates in the cells appear to achieve a greater degree of compactness—and higher E_{FRET} values as a consequence—owing to molecular crowding and confinement by cytoskeleton components and other cellular constituents. However, one should not overinterpret the quantitative distinctions. The difference between E_{FRET} values of 40 and 80% can be accounted for by a small (~30%) change in mean donor-acceptor separation distance or a redistribution of molecular sub-populations. Small changes in orientation and/or ligand saturation (particularly of the acceptor) can also have a large effect on E_{FRET}. Likewise, the E_{FRET} measured for cytoplasmic α-synuclein-C4 may reflect the presence of soluble oligomeric forms of the protein not resolved as distinct structures by microscopy, albeit of great interest due to the attribution of cytotoxicity to such molecular forms[4,5]. Our FRET-based approach may constitute a selective means for monitoring fibril disassembly, a major target of present pharmaceutical research directed at the identification of compounds inhibiting or reversing amyloid deposits.

In conclusion, our results indicate that reliable, direct imaging of α-synuclein aggregation is now possible inside living cells. FRET between FlAsH and ReAsH, and presumably between improved biarsenical FRET pairs reported recently from our laboratories[31], constitutes a valuable reporter of dynamic protein-protein interactions in associated and aggregated forms of α-synuclein. We foresee the utility of α-synuclein-C4 for studying the interaction of α-synuclein with other proteins associated in amyloid aggregates and for screening compounds that inhibit aggregation in vitro and in living cells. Thus, we expect that α-synuclein-C4 may assist

the search for rational therapeutic and preventive measures for Parkinson disease.

METHODS

FlAsH and ReAsH labeling of purified proteins. We expressed α-synuclein and α-synuclein-C4 in PT7.7 vectors in E. coli BL21(DE3) and purified them as previously described[9], adding 2 mM DTT throughout the purification steps to prevent oxidation of cysteine thiols. The protein stocks, dialyzed against 20 mM Na-Hepes (pH 7.2), 2 mM DTT, were stable for 1 year at –80 °C. For biarsenical labeling, we removed DTT by fast-desalting columns (PD-10; Amersham) and immediately labeled the protein with FlAsH or ReAsH at a 1:2 protein/label ratio for 16 h at 4 °C in the dark. Fast-desalting columns equilibrated with 20 mM Na-Hepes (pH 7.2), allowed the removal of unbound dye after the reaction.

Spectroscopic measurements. We performed absorption (A) measurements in a Cary 100 spectrophotometer (Varian), using A_{275} ($\varepsilon_{275} = 5,600$ M^{-1} cm^{-1}) for protein concentration, and extinction coefficients of $\varepsilon_{510} = 55,000$ M^{-1} cm^{-1} for α-synuclein-C4–FlAsH and $\varepsilon_{595} = 13,500$ M^{-1} cm^{-1} for α-synuclein-C4–ReAsH. We measured steady-state fluorescence on a Cary Eclipse spectrofluorimeter (Varian), with λ_{exc} 510 nm/λ_{em} 530 nm for FlAsH and λ_{exc} 595 nm/λ_{em} 610 nm for ReAsH.

We acquired the emission spectra in living HeLa cells (microinjected as described below) with a SpectraCube interferometric spectral analyzer system[26] (Applied Spectral Imaging). Each pixel of SpectraCube collected an interferogram, which was then Fourier transformed to yield the spectrum.

Experiments with cell cultures. We cultured HeLa cells on CellLocate cover slips (Eppendorf) in DMEM containing 4.5 g/l glucose, 10% fetal calf serum and 1% penicillin/streptomycin (complete medium). We microinjected 200 μM α-synuclein-C4–FlAsH or α-synuclein-C4–ReAsH, in serum-free medium Opti-MEM (Invitrogen), using a semi-automatic microinjection apparatus and Femtotips (Eppendorf). The estimated microinjected volume was ~0.1 pl (~1/10 of the cellular volume according to the device manufacturer's guidelines). The typical number of microinjected cells was ~100 (survival rate, ~95%).

We transfected SH-SY5Y human dopaminergic neuroblastoma cells (cultured at 37 °C in 5% CO_2 in complete medium) using 2 μg of plasmid DNA and 5 μl of Lipofectamine 2000 in Opti-MEM (Invitrogen). Three days after transfection, we stained the cells with 1 μM FlAsH (or ReAsH)/10 μM EDT in Opti-MEM, for 2 h at 37 °C and 5% CO_2 in the dark and removed unbound dye by washing with 100 μM EDT in complete medium 4 times for 30 min. We calculated the transfection efficiency on a population of $n > 400$ cells after FlAsH labeling. From the positively transfected cells, we counted the number of them displaying fluorescent aggregates. The data shown represent mean ± s.e.m. of three independent experiments. After staining, we monitored cells for up to 3 d. For stress induction, we incubated the transfected cells with 5–10 mM $FeCl_2$ (Sigma) in complete medium for 2–3 h and stained them with FlAsH 24 h later. We estimated the increase in aggregation arising from the $FeCl_2$ treatment by fluorescence microscopy. From the positively transfected cells, we counted the fraction displaying fluorescent aggregates in the absence and presence of $FeCl_2$. The results represent

mean ± s.e.m. of three independent experiments. The number of cells with aggregates was 8–15 for each replicate, which required a statistical analysis for a small-size population. We evaluated the significance of the difference between these mean values from 95% confidence intervals ($n = 3$ sample set, $\alpha = 0.05$). We then counted the number of aggregates per cell for each sample set and calculated 95% confidence intervals to test significant variations in the mean values for $FeCl_2$-treated and untreated cells.

Nuclear staining with bisbenzimidazole 1 μM Hoechst H33342 in PBS-BSA buffer allowed identification of living HeLa and SH-SY5Y cells, and therefore the recognition of unspecific uptake of FlAsH or ReAsH by dead cells. We incubated the cells at 37 °C for 30 min and placed them in DMEM medium after rinsing with PBS.

Additional methods. Descriptions of plasmid construction, FRET experiments, AFM, NMR spectroscopy, gel electrophoresis, size exclusion chromatography, ThioS staining, aggregation kinetics and immunofluorescence assays are available in **Supplementary Methods**.

Note: Supplementary information is available on the Nature Methods website.

1. Dobson, C.M. Protein folding and misfolding. *Nature* **426**, 884–890 (2003).
2. Dawson, T.M. & Dawson, V.L. Molecular pathways of neurodegeneration in Parkinson's disease. *Science* **302**, 819–822 (2003).
3. Shults, C.W. Lewy bodies. *Proc. Natl. Acad. Sci. USA* **103**, 1661–1668 (2006).
4. Reixach, N., Deechongkit, S., Jiang, X., Kelly, J.W. & Buxbaum, J.N. Tissue damage in the amyloidoses: Transthyretin monomers and nonnative oligomers are the major cytotoxic species in tissue culture. *Proc. Natl. Acad. Sci. USA* **101**, 2817–2822 (2004).
5. Lashuel, H.A. *et al.* Alpha-synuclein, especially the Parkinson's disease-associated mutants, forms pore-like annular and tubular protofibrils. *J. Mol. Biol.* **322**, 1089–1102 (2002).
6. Chandra, S., Gallardo, G., Fernandez-Chacon, R., Schluter, O.M. & Sudhof, T.C. Alpha-synuclein cooperates with CSPalpha in preventing neurodegeneration. *Cell* **123**, 383–396 (2005).
7. Bertoncini, C.W. *et al.* Release of long-range tertiary interactions potentiates aggregation of natively unstructured alpha-synuclein. *Proc. Natl. Acad. Sci. USA* **102**, 1430–1435 (2005).
8. Uversky, V.N., Li, J. & Fink, A.L. Metal-triggered structural transformations, aggregation, and fibrillation of human alpha-synuclein. A possible molecular NK between Parkinson's disease and heavy metal exposure. *J. Biol. Chem.* **276**, 44284–44296 (2001).
9. Hoyer, W. *et al.* Dependence of alpha-synuclein aggregate morphology on solution conditions. *J. Mol. Biol.* **322**, 383–393 (2002).
10. Stefanova, N., Klimaschewski, L., Poewe, W., Wenning, G.K. & Reindl, M. Glial cell death induced by overexpression of alpha-synuclein. *J. Neurosci. Res.* **65**, 432–438 (2001).
11. Sherer, T.B. *et al.* An in vitro model of Parkinson's disease: linking mitochondrial impairment to altered alpha-synuclein metabolism and oxidative damage. *J. Neurosci.* **22**, 7006–7015 (2002).
12. Vila, M. *et al.* Alpha-synuclein up-regulation in substantia nigra dopaminergic neurons following administration of the parkinsonian toxin MPTP. *J. Neurochem.* **74**, 721–729 (2000).
13. Lee, H.J., Shin, S.Y., Choi, C., Lee, Y.H. & Lee, S.J. Formation and removal of alpha-synuclein aggregates in cells exposed to mitochondrial inhibitors. *J. Biol. Chem.* **277**, 5411–5417 (2002).
14. Bence, N.F., Sampat, R.M. & Kopito, R.R. Impairment of the ubiquitin-proteasome system by protein aggregation. *Science* **292**, 1552–1555 (2001).
15. Kim, S., Nollen, E.A., Kitagawa, K., Bindokas, V.P. & Morimoto, R.I. Polyglutamine protein aggregates are dynamic. *Nat. Cell Biol.* **4**, 826–831 (2002).
16. Outeiro, T.F. & Lindquist, S. Yeast cells provide insight into alpha-synuclein biology and pathobiology. *Science* **302**, 1772–1775 (2003).
17. Fortin, D.L. *et al.* Neural activity controls the synaptic accumulation of alpha-synuclein. *J. Neurosci.* **25**, 10913–10921 (2005).
18. Pandey, N., Schmidt, R.E. & Galvin, J.E. The alpha-synuclein mutation E46K promotes aggregation in cultured cells. *Exp. Neurol.* **197**, 515–520 (2006).
19. McLean, P.J., Kawamata, H. & Hyman, B.T. Alpha-synuclein-enhanced green fluorescent protein fusion proteins form proteasome sensitive inclusions in primary neurons. *Neuroscience* **104**, 901–912 (2001).
20. Adams, S.R. *et al.* New biarsenical ligands and tetracysteine motifs for protein labeling in vitro and in vivo: synthesis and biological applications. *J. Am. Chem. Soc.* **124**, 6063–6076 (2002).
21. Gaietta, G. *et al.* Multicolor and electron microscopic imaging of connexin trafficking. *Science* **296**, 503–507 (2002).
22. Arhel, N. *et al.* Quantitative four-dimensional tracking of cytoplasmic and nuclear HIV-1 complexes. *Nat. Methods* **3**, 817–824 (2006).
23. Martin, B.R., Giepmans, B.N., Adams, S.R. & Tsien, R.Y. Mammalian cell-based optimization of the biarsenical-binding tetracysteine motif for improved fluorescence and affinity. *Nat. Biotechnol.* **23**, 1308–1314 (2005).
24. Croisier, E. *et al.* Comparative study of commercially available anti-alpha-synuclein antibodies. *Neuropathol. Appl. Neurobiol.* **32**, 351–356 (2006).
25. Heise, H. *et al.* Molecular-level secondary structure, polymorphism, and dynamics of full-length alpha-synuclein fibrils studied by solid-state NMR. *Proc. Natl. Acad. Sci. USA* **102**, 15871–15876 (2005).
26. Malik, Z. *et al.* Fourier transform multipixel spectroscopy and spectral imaging for quantitative cytology. *J. Microsc.* **182**, 133–140 (1996).
27. Fernandez, C.O. *et al.* NMR of alpha-synuclein-polyamine complexes elucidates the mechanism and kinetics of induced aggregation. *EMBO J.* **23**, 2039–2046 (2004).
28. Matsuzaki, M. *et al.* Histochemical features of stress-induced aggregates in alpha-synuclein overexpressing cells. *Brain Res.* **1004**, 83–90 (2004).
29. Jares-Erijman, E.A. & Jovin, T.M. Imaging molecular interactions in living cells by FRET microscopy. *Curr. Opin. Chem. Biol.* **10**, 409–416 (2006).
30. Egner, A. & Hell, S.W. Fluorescence microscopy with super-resolved optical sections. *Trends Cell Biol.* **15**, 207–215 (2005).
31. Spagnuolo, C.C., Vermeij, R.J. & Jares-Erijman, E.A. Improved photostable FRET-competent biarsenical-tetracysteine probes based on fluorinated fluoresceins. *J. Am. Chem. Soc.* **128**, 12040–12041 (2006).